Materials and Design 45 (2013) 336–342

Contents lists available at SciVerse ScienceDirect

Materials and Design

journal homepage: www.elsevier.com/locate/matdes

Microstructure and fatigue properties of Mg-to-steel dissimilar resistance spot welds

L. Liu [a,b,*], L. Xiao [b], D.L. Chen [c], J.C. Feng [a], S. Kim [d], Y. Zhou [b]

[a] State Key Laboratory of Advanced Welding Production Technology, Harbin Institute of Technology, Harbin 150001, China
[b] Department of Mechanical & Mechatronics Engineering, University of Waterloo, Waterloo, ON, Canada N2L 3G1
[c] Department of Mechanical Engineering, Ryerson University, Toronto, ON, Canada M5B 2K3
[d] Research Institute of Industrial Sci. & Tech., Pohang-si, Gyeongbuk, Republic of Korea

ARTICLE INFO

Article history:
Received 29 February 2012
Accepted 4 August 2012
Available online 30 August 2012

Keywords:
Mg/steel dissimilar welding
Fatigue
Resistance spot welding

ABSTRACT

The structural application of lightweight magnesium alloys in the automotive industry inevitably involves dissimilar welding with steels and the related durability issues. This study was aimed at evaluating the microstructural change and fatigue resistance of Mg/steel resistance spot welds, in comparison with Mg/Mg welds. The microstructure of Mg/Mg spot welds can be divided into: base metal, heat affected zone and fusion zone (nugget). However, the microstructure of Mg/steel dissimilar spot welds had three different regions along the joined interface: weld brazing, solid-state joining and soldering. The horizontal and vertical Mg hardness profiles of Mg/steel and Mg/Mg welds were similar. Both Mg/steel and Mg/Mg welds were observed to have an equivalent fatigue resistance due to similar crack propagation characteristics and failure mode. Both Mg/steel and Mg/Mg welds failed through thickness in the magnesium sheet under stress-controlled cyclic loading, but fatigue crack initiation of the two types of welds was different. The crack initiation of Mg/Mg welds was occurred due to a combined effect of stress concentration, grain growth in the heat affected zone (HAZ), and the presence of Al-rich phases at HAZ grain boundaries, while the penetration of small amounts of Zn coating into the Mg base metal stemming from the liquid metal induced embrittlement led to crack initiation in the Mg/steel welds.
Crown Copyright © 2012 Published by Elsevier Ltd. All rights reserved.

1. Introduction

With increasing use of magnesium alloys in automobile structures due to their high strength-to-weight ratio, dissimilar welding of magnesium alloys to steel has to be considered. It is much more challenging to accomplish magnesium-to-steel (Mg/steel) dissimilar welding than to make magnesium-to-magnesium (Mg/Mg) similar welds, in view of the large differences of electrical/thermal conductivity, thermal expansion coefficient, melting point, etc. [1]. Various methods such as arc [2], friction stir [3], and resistance spot welding [1] have been explored for dissimilar welding of magnesium-to-steel. Good static strength of Mg/steel joints has been achieved, for example, almost 100% shear strength of Mg base material by using a Ni or Cu interlayer [4] and 95% of Mg/Mg spot joint strength by using resistance spot welding [1]. The question arose if the fatigue performance of Mg/steel dissimilar welds would also be acceptable since, to the authors' knowledge, no such studies have been reported in the open literature so far.

Only a few publications on the fatigue strength of other material combinations are available in the open literature; usually it has been reported that the fatigue strength of dissimilar welds is much lower than that of base metals and similar welds. For example, the fatigue strength of butt joined aluminum-to-steel (Al/steel) welds was reported to be 30% lower than aluminum base metal [5]. The fatigue strength of friction stir spot welded Al/steel was about half that for comparable Al/Al spot welds [6,7]. It is believed that brittle intermetallic layers are the main reason for poor dissimilar joint performance because fatigue failure of dissimilar welds always occurred at the interface where intermetallic compounds were formed, which typically have a low critical stress intensity factor and fast crack propagation rate [6].

The objective of the present work was, therefore, to evaluate the microstructure and fatigue properties of Mg/steel dissimilar welds and identify the underlying fracture mechanisms. The fatigue properties of Mg/Mg welds were also determined in the present study for the purpose of comparison.

2. Experimental procedure

The material used in this study was a strip cast AZ31B Mg alloy and hot-dip galvanized HSLA steel, with a thickness of 1.5 mm and 0.77 mm, respectively. The selected thinner steel was aimed to

* Corresponding author at: Department of Mechanical & Mechatronics Engineering, University of Waterloo, Waterloo, ON, Canada N2L 3G1. Tel.: +1 519 888 4567x35625.
E-mail address: rayliu@uwaterloo.ca (L. Liu).

0261-3069/$ - see front matter Crown Copyright © 2012 Published by Elsevier Ltd. All rights reserved.
http://dx.doi.org/10.1016/j.matdes.2012.08.018

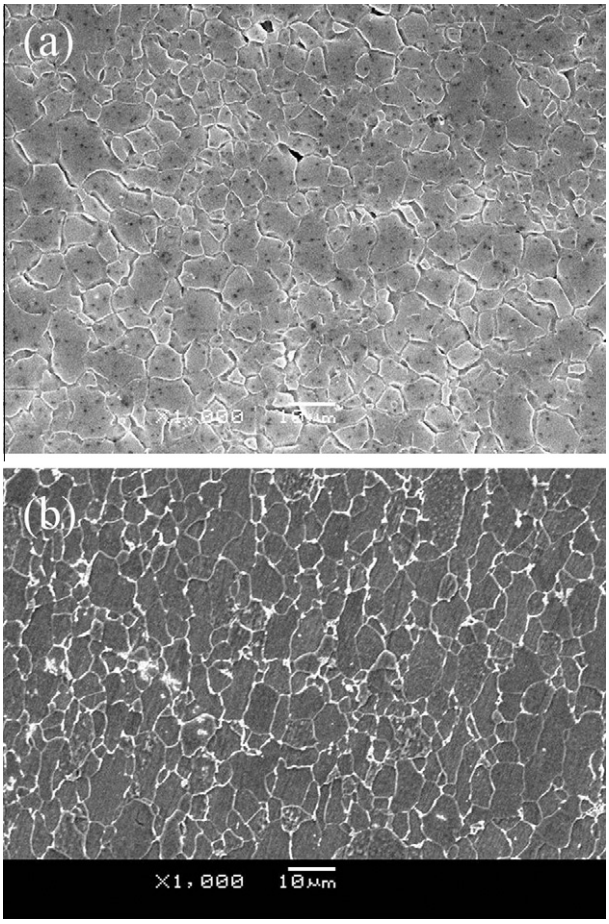

Fig. 1. Microstructures of base materials selected in the present study: (a) AZ31 and (b) HSLA.

reduce the heat generation and increase the heat flow of steel side. The microstructures of the Mg and steel base materials are shown in Fig. 1a and b, respectively. The AZ31 alloy consisted of equiaxed grains. The HSLA steel had a fine-grained ferrite matrix with dispersed carbides at the grain boundaries. The average coating weight of the HSLA steel was 77 g/m^2 (~11 μm in thickness).

Lap welded joints were made by assembling test coupons which were cut to approximately 25 mm width and 100 mm length according to the American Welding Society (AWS) standard D 17.2 [8]. Specimens were ultrasonically cleaned for 5 min in acetone. Prior to welding the surfaces of the Mg coupons were further cleaned with a solution of 2.5% (w/v) chromic acid to minimize surface oxides. Specimens were welded using a MFDC resistance spot welding machine (a product of Centerline Ltd.) in the constant current mode. The configuration of the welds is shown in Fig. 2a. Symmetrical electrode caps (FF25) with a sphere radius of 50.8 mm and face diameter of 16 mm were used for welding Mg/Mg. Asymmetrical electrodes, with a FF25 electrode cap against the Mg side and a flat face electrode against the steel, were used for Mg/steel to balance the workpiece heating by reducing the current density and increasing the cooling rate of the steel sheet.

Fatigue tests were conducted using an Instron 8874 servo-hydraulic fatigue testing system in a load-control mode at a load ratio of $R = 0.2$. The test frequency was between 2 and 30 Hz depending on the load level. The failure criterion was set as final separation of test coupons or the tests were stopped at a number of 10^7 cycles if no failure occurred. Two spacers corresponding to the thickness of the other end were used to compensate for coupon offset and prevent the initial bending during the tests.

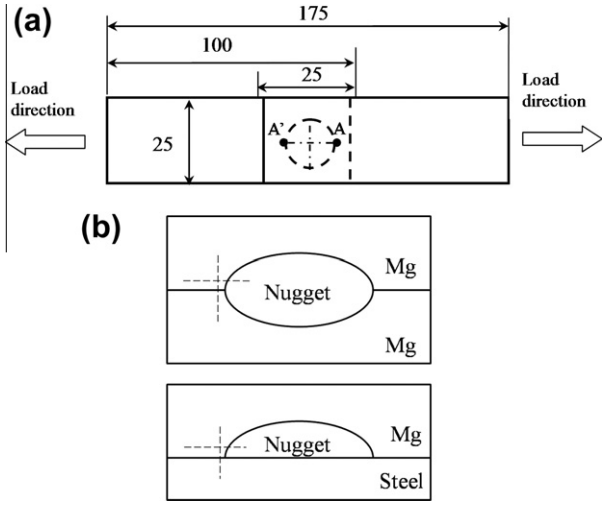

Fig. 2. Schematic diagrams of tensile test and spot welds: (a) configuration of resistance spot welded test coupons and (b) schematic diagram of Mg/Mg and Mg/steel spot welds.

The fracture surface morphology and microstructures were examined by an optical microscope, and a JEOL JSM-6460 scanning electron microscope (SEM) equipped with an Oxford energy-dispersive spectrometer (EDS). The metallographic samples were sectioned across the weld centre parallel to the loading direction, and then hot mounted at 120 °C, ground, polished and etched with a solution of 4.2 g picric acid, 10 ml acetic acid, 70 ml ethanol, and 10 ml water. The nugget size was measured by etching the cross section of the welded samples. Samples after fatigue tests were cross-sectioned along the loading direction and through the weld center as well. The microhardness profiles of the welds were measured on the cross-sections using a LECO MHT-200 Vickers microhardness apparatus, with a load of 100 g and a holding time of 15 s.

Fig. 2b shows the schematic diagram of Mg/Mg and Mg/steel spot welds. The Mg/Mg weld had a systemic nugget (fusion zone) at both upper and lower welded sheets. In the Mg/steel weld, the steel did not melt; the Mg melted and formed a nugget on the steel surface. The dashed lines indicate hardness profile testing position. The horizontal test lines were close to the faying surface where fatigue crack initiation occurs because of the stress concentration [7]. The vertical test line was positioned outside of the fusion zone and close to the notch where cracks have been found to propagate [7].

3. Results

3.1. Microstructure and microhardness

Figs. 3 and 4 show the microstructures of as-welded Mg/Mg and Mg/steel. For the Mg/Mg spot weld as shown in Fig. 3, Al rich phases at grain boundaries were observed both in the nugget (or fusion zone, FZ) and heat affected zone (HAZ), which was the brighter area as confirmed by EDS analysis. This was commonly observed in other AZ31 Mg welds made by other welding methods, such as arc and laser welding, which is related to microsegregation and constitutional liquation [9,10]. However, Al rich phases in AZ31B Mg base material were barely visible under SEM, as shown in Fig. 1a, which is because those Al rich phases were dissolved into matrix during the heat treatment of sheet processing [11].

As discussed in our previous study [1], the microstructure of Mg/steel dissimilar spot welds could be divided into three different regions along the interface of the joined area from center to outside (from right to left in Fig. 4a): weld brazing (magnesium alloy was melted and brazed to steel), solid-state joining (magnesium to

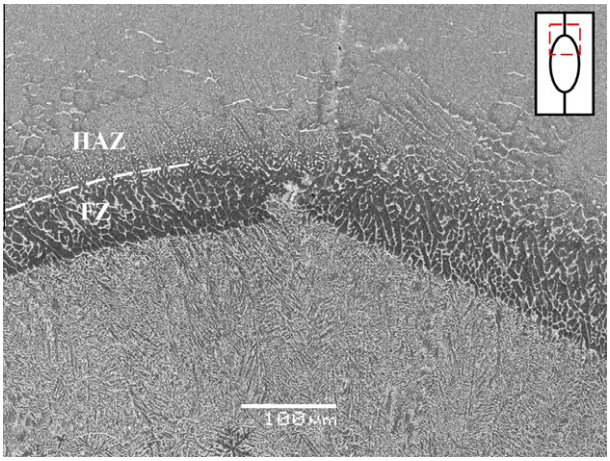

Fig. 3. Microstructure of Mg/Mg weld.

steel), and soldering (Zn as solder). No continuous intermetallic layer was observed in the interface of solid state and weld brazing region under SEM examination as shown in Fig. 4b, which may be the reason that the joint strength was comparable to Mg/Mg welds. In contrast, interfaces with a micro-scale intermetallic layer, such as Al/steel joints, have low fatigue strength [12]. It is interesting to note that in the soldered region the zinc penetrated into the magnesium base material along the grain boundaries (Fig. 4a and c). Table 1 shows the chemical compositions of the soldering areas as determined via EDS analysis. The soldering layer had a chemical composition of about 52 at% Mg, 42 at% Zn and 6 at% Al, and the Zn penetrated region had about 92 at% Mg, 6 at% Zn and 2 at% Al.

Fig. 5a and b show the hardness distribution along the tensile loading direction of Mg/Mg and Mg/steel welds, respectively. The fusion line was positioned at 0 mm. The Mg side of the Mg/steel weld had a similar hardness profile and values as in the Mg/Mg weld, i.e., the lowest hardness appeared in the nugget and the highest in the base metal. At the steel side of the Mg/steel weld the hardness showed a progressive increase in local hardness moving outwards from left to right. This may be due to the formation of martensite islands during cooling [13]. Fig. 5c shows the hardness profile along the thickness direction. The hardness profile of the Mg side in the Mg/steel welds was also similar to that of Mg/Mg with an average of about HV 65. The hardness of the steel side was above HV 140, with the highest hardness appearing near the center where the martensite transformation occurred [1]. In short, the horizontal and vertical Mg hardness profiles of Mg/steel and Mg/Mg welds were similar. The hardness of steel in Mg/steel was more than twice that of Mg.

3.2. Failure mode and fatigue strength

Figs. 6 and 7 show typical cross-section images of failed Mg/Mg and Mg/steel samples fatigued at a 2.0 kN maximum cyclic load, respectively. For the Mg/Mg weld as shown in Fig. 6, fatigue cracks mostly propagated into the Mg base metal from both loading ends. It was found, as shown in Fig. 6b and c that fatigue cracking either initiated at the HAZ, or hundreds of micrometers away from the nugget edge. FEA modeling showed that maximum von Mises stress did not occur right at the notch but about 0.2 mm away from the notch [14]. Therefore, crack initiation sites were determined by the combined effect of stress concentration, grain growth in HAZ, and Al rich phases at the HAZ.

The cracking in Mg/steel welds started at the notch root of both steel and Mg ends but propagated along different directions, as shown in Fig. 7a and b, respectively. At the Mg end, a crack propagated into the Mg base metal until failure occurred. At the

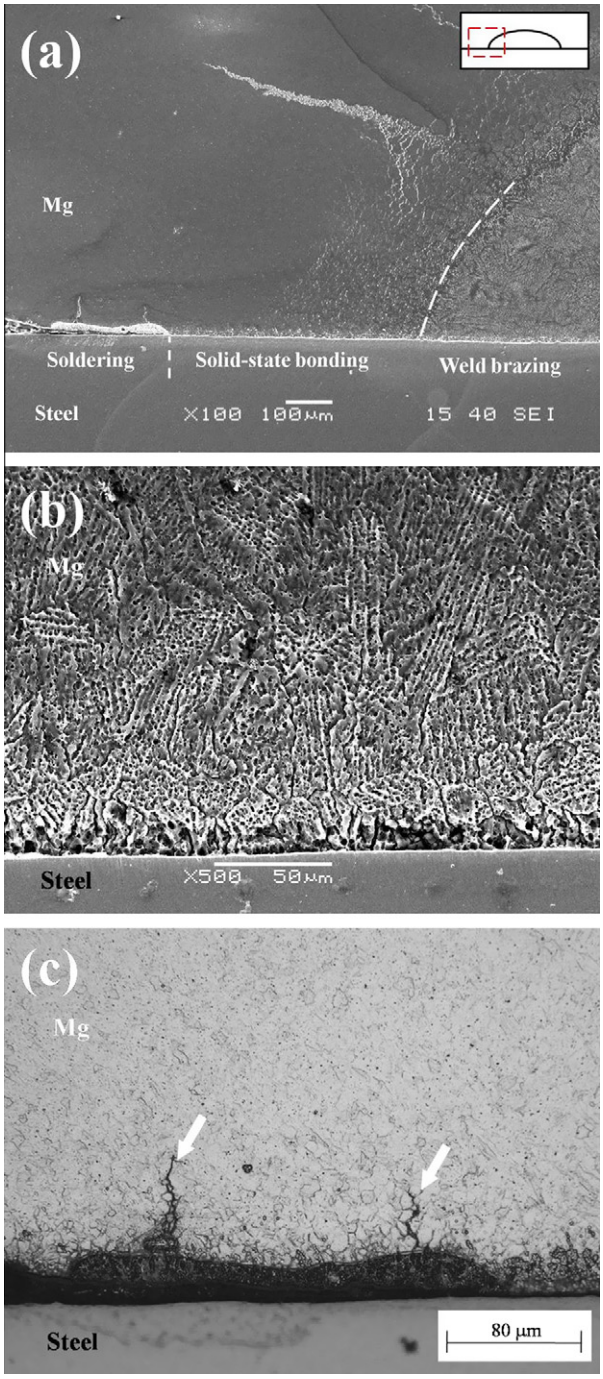

Fig. 4. Microstructure of Mg/steel weld: (a) Mg/steel; (b) higher magnification image of weld brazing region in (a); and (c) higher magnification image of soldering region, with Zn penetrated on Mg side in (a).

Table 1
Elemental composition of different points in Fig. 4a, in at%.

Area	Mg	Al	Fe	Zn
Soldered zone	52	6	–	42
Zn penetration	92	2	–	6

steel end, the crack only propagated along the Mg and steel interface into the nugget for a distance of 400–500 μm, which is much smaller than the nugget size (9.4 mm). This indicates that the crack propagation rate of the Mg and steel interface was much lower

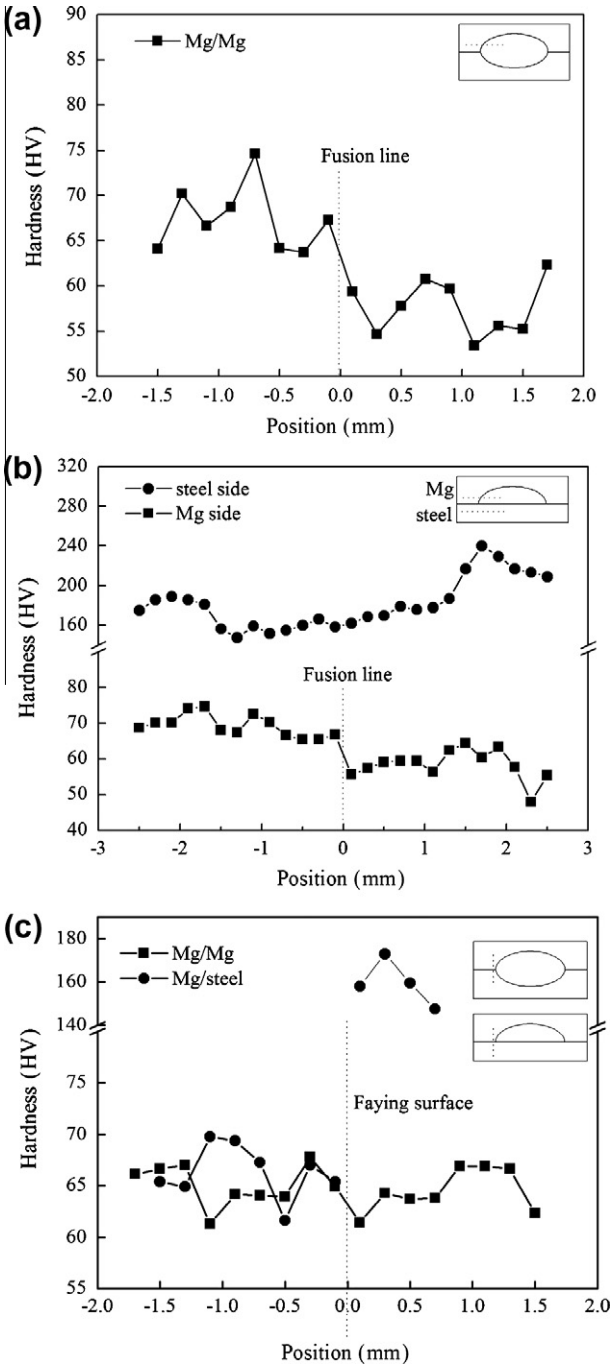

Fig. 5. Hardness profiles of Mg/Mg similar and Mg/steel dissimilar welds: (a) Mg/Mg, parallel to the loading direction; (b) Mg/steel, parallel to the loading direction; and (c) Mg/Mg and Mg/steel, normal to the loading direction.

than that of the Mg base metal, confirming better joint strength of the Mg/steel weld interface.

Fig. 8a shows the maximum cyclic load vs fatigue life of spot welded specimens, in which the nugget diameter of Mg/Mg and Mg/steel welds was 7.8 and 9.4 mm, respectively. It seems the fatigue life of the Mg/steel weld was longer than that of the Mg/Mg weld, and the difference between them decreased with decreasing maximum load (recorded in the semi-log coordinate) when keeping the load ratio constant ($R = 0.2$). However, since the nugget size could change the stress distribution which is directly related to the fatigue properties of spot welds [15], the fatigue strength of similar and dissimilar welds may not be simply compared on the basis of Fig. 8a.

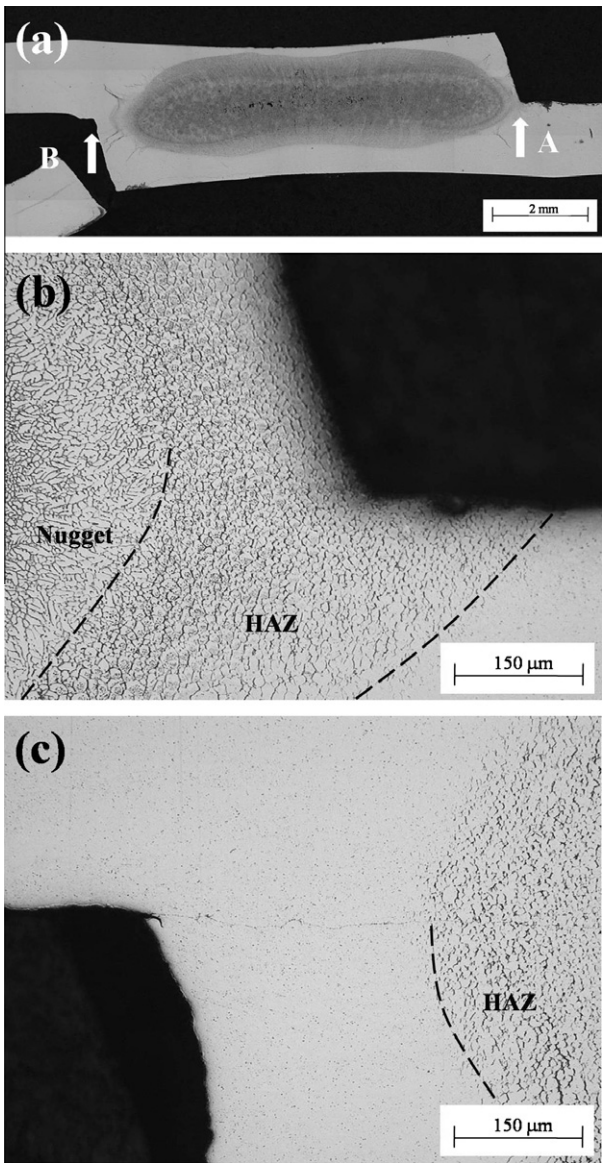

Fig. 6. Mg/Mg spot weld after fatigue test at a maximum load of 2.0 kN: (a) overall view; (b) higher magnification image of crack initiation site A; and (c) higher magnification image of crack initiation site B.

The high cycle fatigue failure mode of both Mg/steel and Mg/Mg welds was through thickness (Figs. 6 and 7), in which the primary cracks initiated outside of the nugget and propagated into the Mg base metal through-thickness. It follows that the failure mechanism at the microstructural level was in fact dominated by tensile fracture [16]. The distribution of the tensile stress around the nugget can be simplified as [16],

$$\sigma(\theta) = \sigma_{\max} \cdot \cos\theta, \tag{1}$$

where θ is from $-90°$ to $90°$ and $\sigma_{\max}$ is the maximum tensile stress occurring at $\theta = 0°$. It should be noted that both Mg/Mg and Mg/steel samples barely rotated during high fatigue tests with proper spacers added in the clamping area. Therefore, the stiffness difference between Mg and steel could be ignored. Then the applied tensile load P becomes [16],

$$P = \int_{-\pi/2}^{\pi/2} \sigma(\theta) \cdot \frac{d}{2} t \cdot \cos\theta \cdot d\theta = \frac{\pi}{4} t d \sigma_{\max} = 0.785 t d \sigma_{\max}, \tag{2}$$

where t is thickness, d is nugget diameter, and $\sigma_{\max}$ is the maximum stress around the nugget. Re-arranging Eq. (2) yields [16],

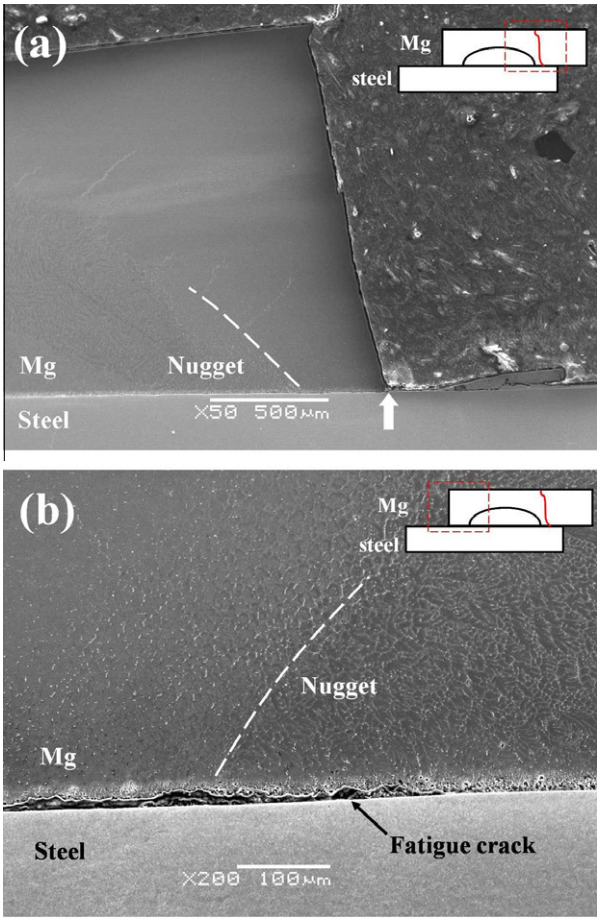

Fig. 7. Mg/steel spot weld after fatigue test at a maximum load of 2.0 kN: (a) Mg end; (b) steel end.

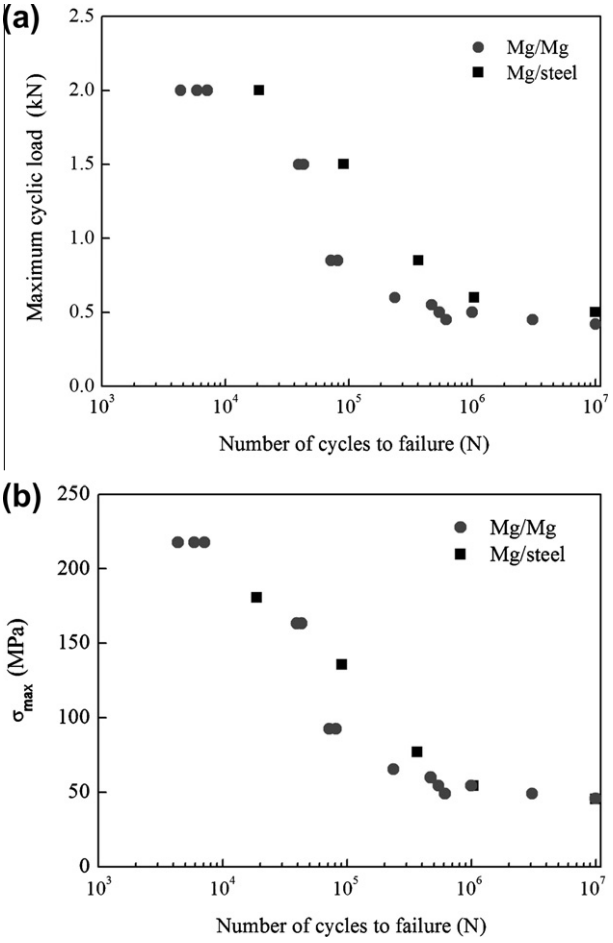

Fig. 8. Fatigue life data of similar Mg/Mg and dissimilar Mg/steel spot welds: (a) the maximum load vs number of cycles to failure and (b) the normalized maximum stress vs number of cycles to failure.

$$\sigma_{max} = \frac{P}{0.785td}. \quad (3)$$

In the present study t should be 1.5 mm because both similar and dissimilar welds failed at the Mg side. σ_{max} should be positioned in A and A' in Fig. 2a where the crack initiated. The maximum cyclic load shown in Fig. 8a could then be "normalized" by using σ_{max} to better compare the similar and dissimilar welds. As shown in Fig. 8b, the "normalized" fatigue curves of dissimilar and similar welds were similar. Thus good fatigue resistance was obtained for the current dissimilar welds in contrast to the usual behavior in which the fatigue strength of dissimilar welds was much lower than similar welds [6,7].

3.3. Fractography

Figs. 9 and 10 show typical images of fracture surfaces of Mg/Mg and Mg/steel weld fatigued at a maximum cyclic load of 0.85 kN, respectively. In general, fatigue fracture surfaces can be divided into three regions: crack initiation, crack propagation and final rapid failure. Fatigue crack initiation occurred either from the surface (Fig. 9b) or a sub-surface defect (Fig. 9c). The initiation site of Mg/Mg weld comprised 95 wt% Mg and 5 wt% Al via EDS analyses. The Al content at the fatigue initiation site was observed to be higher than that of the base metal, suggesting that Al rich phases (mostly β-$Al_{12}Mg_{17}$, as shown in Fig. 3) formed at the grain boundary of HAZ during the high temperature process of welding. It has been proved that the $Al_{12}Mg_{17}$ along the grain-boundaries has a negative influence on ductility and fracture toughness of Mg–Al alloys [17]. Therefore, the Al rich grain boundaries usually acted as fatigue initiation sites. The morphology of the propagation areas C (close to initiation site) and D (at the middle of the coupon width, close to Mg coupon surface) were almost the same, which were mainly characterized by fatigue striations (Fig. 9d). This suggests that cracks propagated with relatively lower speed at least until reaching the surface of the specimen. Out of the width direction, final rapid propagation areas exhibited a tensile-like fracture surface feature since they were characterized by dimples, as shown in Fig. 9e. This was due to the fact that the load-carrying capacity of the final remaining ligament/cross-section was exhausted at the final stage of fatigue crack propagation.

Only a surface initiation mode was observed in Mg/steel welds (Fig. 10a). The crack initiation site of Mg/steel contained more Zn with a chemical composition of 57 wt% Mg and 43 wt% Zn. The crack propagation characteristics of the Mg/Mg welds were similar to those of Mg/steel welds as shown in Fig. 10b suggesting that the propagation processes of Mg/Mg and Mg/steel would be similar since both proceeded in the Mg coupon.

According to the fracture morphologies shown in Figs. 9 and 10, the primary crack propagation of both Mg/steel and Mg/Mg spot welds could be divided into three stages, as schematically illustrated in Fig. 11. In stage I, cracks propagated along both the sheet thickness and width directions at a relatively low rate. The fracture morphology can be characterized as fatigue striations (Figs. 9d and 10b). The fatigue propagation ended until visible cracks reached the top and/or bottom of the specimen surface, but the two sheets were not separated, as shown in Fig. 11b, stage II. In stage III, cracks propagated along the width direction until the sample was broken into two parts. No fatigue striations could be

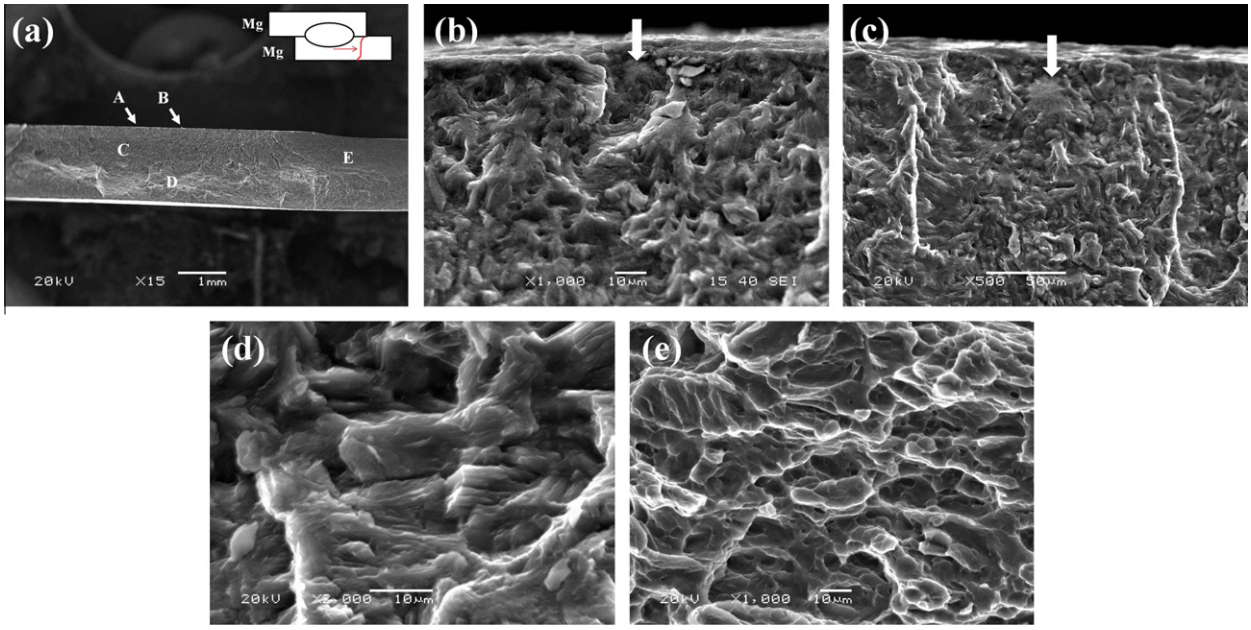

Fig. 9. Fracture surface morphology of Mg/Mg weld tested at a maximum cyclic load of 0.85 kN: (a) overall view; (b) surface crack initiation site (area A); (c) subsurface crack initiation site (area B); (d) typical image of propagation region (area C and D); (e) fast propagation region (area E).

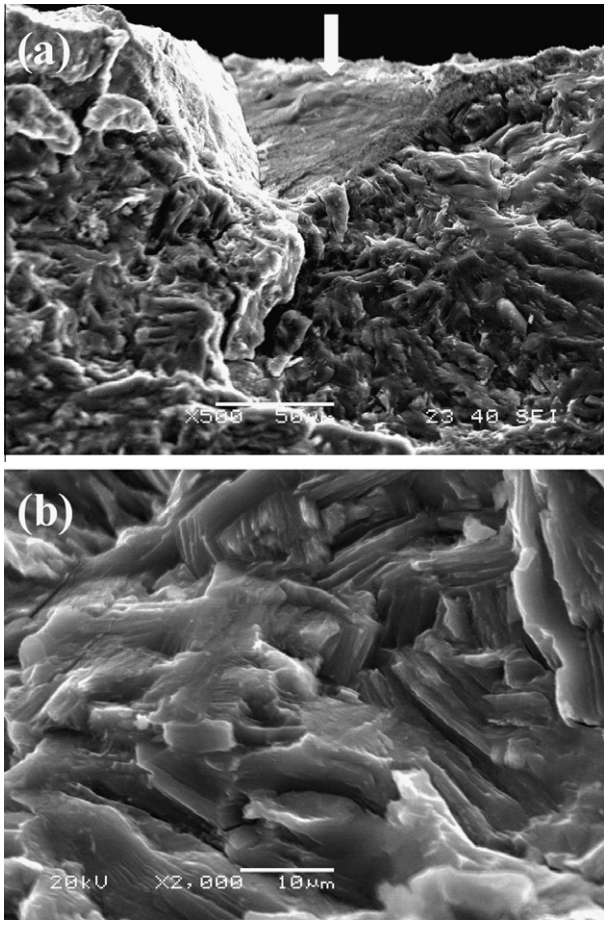

Fig. 10. Fracture surface morphology of Mg/steel dissimilar weld tested at a maximum cyclic load of 0.85 kN: (a) crack initiation site and (b) typical crack propagation region.

observed in this region, where the propagation rate was fairly high, corresponding to the final rapid propagation stage.

4. Discussion

4.1. Liquid metal induced embrittlement

The Liquid Metal Induced Embrittlement (LMIE) refers to the loss of ductility of normally ductile metals and alloys when stressed while in contact with a liquid metal [18]. The study on the occurrence of LMIE in the Mg–Zn couple is limited, but many investigations have been done for the Fe–Zn couple and several suggested mechanisms of LMIE have been reported, such as pre-existing cracks, stress-assisted dissolution, and the weakening of interatomic bonds by the presence of a liquid metal at the crack tip. The susceptibility to LMIE is related to chemistry of couples, grain size, grain boundary chemistry, residual stress or dislocation density, exposure conditions, etc. [19].

During welding, the liquid Zn was in contact with Mg and steel sheets and penetrated into the Mg along grain boundaries. The observed crack initiation sites of Mg/steel welds showed an intergranular fracture surface and contained around 50 wt% Zn which corresponds to the soldered region in Fig. 4a and c. So crack initiation of dissimilar welds was a typical LMIE which was caused by penetrated Zn. In terms of the ductility and fatigue strength, the LMIE of the Mg–Zn couple should be more damaging than the grain boundary segregation of the Mg–Al couple because the Mg–Zn intermetallic intergranular layer was wider and distributed continuously while the segregation of Mg–Al was narrow and distributed discontinuously along the grain boundaries. It also means that the crack initiation time of Mg/steel welds should be less than that of Mg/Mg welds. However, since the welding time was only 0.13 s, the Zn evidently had not enough time to penetrate deeply into the surface. This can be seen in Figs. 4c and 10a, where the penetration depth of the LMIE was 30–60 μm, being less than 4% of the sheet thickness.

At less than 450 °C, Zn penetration can be observed in both steels and Mg alloys [20]. The current observation of Zn penetration occurring only in Mg suggests that the Zn–Mg couple was more susceptible to LMIE than the Zn–Fe couple. It also suggests that specific attention should be paid when Zn based filler metal is used to braze/solder Mg alloys.

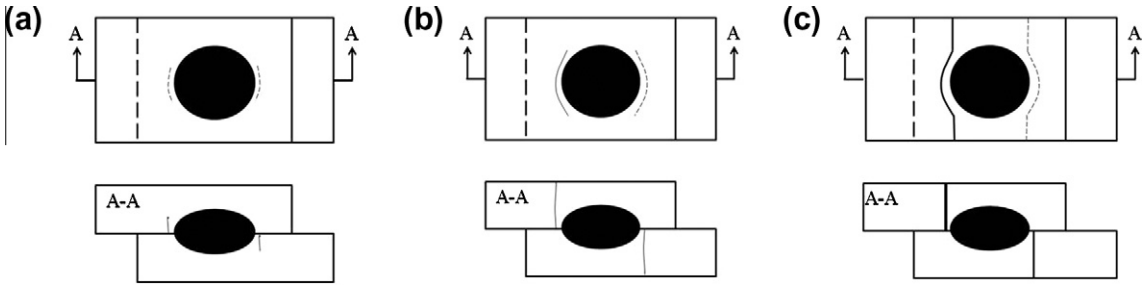

Fig. 11. Schematic illustration of fatigue failure process. (a) stage I, cracks propagated around the nugget outer-area and though the thickness; (b) stage II, visible cracks appeared at the center of the top or bottom specimen surface, but the two sheets were not separated; and (c) stage III, cracks propagated along the sheet width direction until two sheets were separated.

4.2. Fatigue life

Due to the special geometry of the spot welds, it is hard to determine the crack initiation life and propagation rate. Copper and Smith [21] applied a direct voltage between the nugget and clamped coupon in order to measure the crack propagation rate online, and observed that cracks initiated almost at the onset of the test and thus macrocrack propagation dominated the fatigue lives of the order of 2×10^6 cycles. In contrast, McMahon et al. [22] measured crack propagation length of half-sectioned nuggets and concluded that crack initiation occupied a significant part of the fatigue life. In the present case of comparing Mg/steel and Mg/Mg spot welds, in spite of different crack initiation sites, similar crack propagation mechanisms were observed (Figs. 9 and 10), and similar fatigue life was obtained after the nugget size and sheet thickness were taken into consideration based on Eq. (3), as shown in Fig. 8b. This suggests that the majority of fatigue life would be spent in crack propagation. Further studies in this aspect are needed to confirm this deduction.

5. Conclusions

The Microstructure and fatigue properties of Mg-to-steel dissimilar resistance spot welds were evaluated in this study, in comparison with Mg/Mg welds. The main conclusions are as follows:

(1) The Mg/steel dissimilar welds showed almost the same fatigue performance as the Mg/Mg similar welds.
(2) The crack initiation of Mg/Mg welds occurred basically from the HAZ. Both stress concentration and weakening in the HAZ were responsible for the initiation of Mg/Mg welds. The Mg/steel welds appeared to exhibit only surface crack initiation which was attributed to the presence of liquid metal induced embrittlement in the Mg–Zn couple arising from the squeezed out liquid Zn during welding. The penetration depth of the LMIE was less than 4% of the sheet thickness and caused no obvious reduction in the fatigue propagation life.
(3) Similar fatigue crack propagation path and characteristics were observed in both types of Mg/Mg and Mg/steel spot welds, leading to equivalent fatigue lives of the similar and dissimilar spot welds.

Acknowledgments

This research was financially supported by the Natural Sciences and Engineering Research Council (NSERC) of Canada, AUTO21 Network Centres of Excellence of Canada, and NSERC Magnesium Network (MagNET). The authors want to thank Dr. Y. Ding and X. Li, Profs. S. Lawson, G.S. Zou and L.Q. Li for their suggestions in this work, and the materials support from POSCO.

References

[1] Liu L, Xiao L, Feng JC, Tian YH, Zhou SQ, Zhou Y. The mechanisms of resistance spot welding of magnesium to steel. Metall Mater Trans A 2010;41:2651–61.
[2] Liu LM, Wang SX, Zhu ML. Study on TIG welding of dissimilar Mg alloy and Cu with Fe as interlayer. Sci Technol Weld Joining 2006;11:523–5.
[3] Liyanage T, Kilbourne J, Gerlich AP, North TH. Joint formation in dissimilar Al alloy/steel and Mg alloy/steel friction stir spot welds. Sci Technol Weld Joining 2009;14:500–8.
[4] Liu L, Qi X. Strengthening effect of nickel and copper interlayers on hybrid laser-TIG welded joints between magnesium alloy and mild steel. Mater Des 2010;31:3960–3.
[5] Uzun H, Dalle Donne C, Argagnotto A, Ghidini T, Gambaro C. Friction stir welding of dissimilar Al 6013-T4 to X5CrNi18-10 stainless steel. Mater Des 2005;26:41–6.
[6] Tran VX, Pan J. Fatigue behavior of dissimilar spot friction welds in lap-shear and cross-tension specimens of aluminum and steel sheets. Int. J. Fatigue 2010;32:1167–79.
[7] Chang BH, Du D, Sui B, Zhou Y, Wang Z, Heidarzadeh F. Effect of forging force on fatigue behavior of spot welded joints of aluminum alloy 5182. J Manuf Sci Eng 2007;129:95–100.
[8] AWS D 17.2, Specification for resistance welding for aerospace applications, American Welding Society; 2007.
[9] Cao X, Jahazi M, Immarigeon JP, Wallace W. A review of laser welding techniques for magnesium alloys. J Eng Mater Technol 2006;171:188–204.
[10] Munitz A, Cotler C, Stern A, Kohn G. Mechanical properties and microstructure of gas tungsten arc welded magnesium AZ91D plates. Mater Sci Eng A 2001;302:68–73.
[11] Chen H, Kang SB, Yu H, Kim HW, Min G. Microstructure and mechanical properties of Mg-4.5 Al-1.0 Zn alloy sheets produced by twin roll casting and sequential warm rolling. Mater Sci Eng A 2008;492:317–26.
[12] Qiu R, Shi H, Zhang K, Tu Y, Iwamoto C, Satonaka S. Interfacial characterization of joint between mild steel and aluminum alloy welded by resistance spot welding. Mater Charact 2010;61:684–8.
[13] Khan MI, Kuntz ML, Biro E, Zhou Y. Microstructure and mechanical properties of resistance spot welded advanced high strength steels. Mater Trans 2008;49:1629–37.
[14] Wang G, Barkey ME. Investigating the spot weld fatigue crack growth process using X-ray imaging. Weld J 2006:85.
[15] Zhang S. Stress intensities at spot welds. Int J Fract 1997;88:167–85.
[16] Chao YJ. Ultimate strength and failure mechanism of resistance spot weld subjected to tensile, shear, or combined tensile/shear loads. J Eng Mater Technol 2003;125:125–32.
[17] Yakubtsov IA, Diak BJ, Sager CA, Bhattacharya B, MacDonald WD, Niewczas M. Effects of heat treatment on microstructure and tensile deformation of Mg AZ80 alloy at room temperature. Mater Sci Eng A 2008;496:247–55.
[18] Fernandes PJL, Jones DRH. Mechanisms of liquid metal induced embrittlement. Int Mater Rev 1997;42:251–61.
[19] Nicholas MG, Old CF. Review liquid metal embrittlement. J Mater Sci 1979:14.
[20] Shunk F. Specificity as an aspect of liquid metal embrittlement. Scripta Metall 1974;8:519–26.
[21] Cooper JF, Smith RA. The measurement of fatigue cracks at spot-welds. Int J Fatigue 1985;7:137–40.
[22] McMahon JC, Smith GA, Lawrence FV. Fatigue crack initiation and growth in tensile-shear spot weldments. In: McHenryJ HI, Potter M, editors. Fatigue and fracture testing of weldments. Philadelphia: American Society for Testing and Materials; 1990. p. 47–77